FEATURE ARTICLE

Magnetic Interactions of Iron Nanoparticles in Arrays and Dilute Dispersions

Dorothy Farrell,[†,‡] Yuhang Cheng,[†] R. William McCallum,[§] Madhur Sachan,[†] and Sara A. Majetich*[,†]

Physics Department, Carnegie Mellon University, Pittsburgh, Pennsylvania 15213-3890, London Centre for Nanotechnology, University College London, London, WC1E 7HN, UK, and Ames Laboratory, Iowa State University, Ames, Iowa 50011

Received: January 10, 2005; In Final Form: May 11, 2005

The magnetic properties of monodisperse Fe nanoparticles with over 4 orders of magnitude difference in concentration are studied by a combination of ordinary and remanent hysteresis loops, zero field cooled magnetization as a function of temperature, and magnetic relaxation rates. We compare the behavior of dilute dispersions with different concentrations, dispersions, and arrays made from the same particles, and nanoparticle arrays with different particle sizes and separations. The results are related to theoretical predictions and are used to create a unified picture of magnetostatic interactions within the assemblies.

Introduction

Monodisperse monodomain magnetic nanoparticles[1−5] are an ideal system for studying magnetostatic interactions, since they act like giant magnetic moments. There have been numerous studies of these nanoparticles in ferrofluids,[5−19] where the particle concentration is a few volume percent or less, and also in self-assembled nanoparticle arrays,[20−26] where the volume fraction is limited only by the thickness of the surfactant coating.

Magnetostatic forces are long-range and have subtle effects. These have been documented by studying the peak temperature in the imaginary susceptibility as a function of frequency over 5 orders of magnitude as a ferrofluid is diluted.[8] Dilute ferrofluids have also been shown to behave like dipolar spin glasses.[9] In a more concentrated assembly, where the interactions are stronger, it is theoretically possible to have a purely dipolar ferromagnet. For a two-dimensional hexagonal lattice of point dipoles, the magnetic ground state is ferromagnetic, but for a square lattice, the minimum energy configuration has alternating rows of aligned spins.[27] It is therefore interesting to see if the interactions in nanoparticle arrays are sufficiently strong to test these predictions at finite temperatures.

Different groups have reported conflicting results on whether the coercivity, remanence, and relaxation rate go up or down with increasing particle concentration.[19] The self-assembled nanoparticle arrays show some collective behavior, but the magnetostatic forces that cause it are weak and long range, compared with the exchange forces that couple atomic spins within a particle. It is unclear under what conditions mean field theories based on dipolar interactions will be valid, or on what length scale Landau-Lifschitz-Gilbert modeling of magnetization dynamics beaks down due to the granularity of the particle assemblies.

Here we describe how the magnetic properties of monodisperse Fe nanoparticles are modified by changing the particle concentration and particle size. Unlike previous studies, we study similar particles with over 4 orders of magnitude difference in the volume fraction, ranging from highly dilute dispersions to close-packed arrays. Because of the surfactant coating, the particle assemblies can have high density without exchange coupling between particles that would otherwise dominate the magnetic properties. The goal of this work is to develop an improved understanding of the magnetization pattern within a

Sara Majetich received an A. B. in chemistry at Princeton University, and a Masters Degree in Physical Chemistry at Columbia University. She earned a Ph.D. in Solid State Physics from the University of Georgia and did postdoctoral work at Cornell University before joining the faculty at Carnegie Mellon University in 1990. She is the recipient of a National Young Investigator Award from the NSF. More about the Majetich group research can be found at http://www.andrew.cmu.edu/user/sm70/index.html.

* Corresponding author. E-mail: sm70@andrew.cmu.edu.
[†] Carnegie Mellon University.
[‡] University College London.
[§] Iowa State University.

10.1021/jp050161v CCC: $30.25
Published on Web 06/23/2005

dense nanoparticle assembly, through macroscopic measurements of the magnetization as a function of the applied field, temperature, and time.

Experimental Methods

A. Sample Preparation and Structure. Monodisperse Fe nanoparticles 4.5 to 9.3 nm in diameter were prepared under an argon atmosphere via thermal decomposition of iron pentacarbonyl, $Fe(CO)_5$, using a heterogeneous nucleation technique that has been reported elsewhere.[32] To vary the particle size, an additional stage of growth followed. The volume of octyl ether was doubled to reduce the concentration of particles in solution and heating began again. $Fe(CO)_5$ was again added at 100 °C, and heating continued until 260 °C, after which the sample was cooled and removed to an argon atmosphere glovebox for washing. Reactions were done with and without a 1:1 molar ratio mixture of oleic acid (OA) and oleylamine (OY) present. The surfactant binds to the Fe particle surface and provides a barrier against agglomeration. OA is used for strong binding to the Fe surface, and OY is mixed with OA to reduce the oxidation reactivity of the OA. The molar ratio of the first stage Fe to surfactant in these syntheses was varied between 2.2:1 and 4.6:1, treating each OA/OY pair as a single molecule. Assuming a headgroup area of 0.25 nm^2 for OA and OA/OY mixes, comparisons of surfactant concentration (15−45 mM) and particle concentration indicate that surfactant concentration is greater than that needed to coat the surfaces of the particles. The samples were washed by adding ethanol in a 3:1 volume ratio to the octyl ether, causing the particles to aggregate. The aggregates were then collected with a magnet, the supernatant was decanted, and hexane added to redisperse the particles. Surfactant was added at a concentration of 15 to 45 mM during each washing stage. The hexane suspensions were typically 2−20 times more dilute than the original octyl ether suspensions.

Since the surfactant chain provides the steric repulsion that keeps particles separated even in a dried state, the interparticle spacing in dried assemblies of particles can be reduced by exchanging surfactants. A mixture of hexanoic acid (HA), C_5H_{11}-COOH, and hexylamine (HY), $C_6H_{13}NH_2$ was used as a replacement short chain surfactant. The shorter chain length of these molecules results in smaller surfactant volume, allowing them to penetrate the larger surfactant coating and displace the larger molecules. Like OA and OY, HA and HY reacted upon mixing, and were therefore also considered to be a double-chained surfactant in the mixed state.

The as-made particle concentrations of the samples were determined from calibrated X-ray fluorescence.[32] The energies of the emitted X-rays are specific to the elements in the sample, and the relative concentrations of the elements are determined by pattern intensities. The results indicate a roughly 40% yield for the synthesis, based on the initial amount of $Fe(CO)_5$ and the average particle size found from TEM. These results were used to estimate the concentrations of the hexane dispersions made from them. The particle arrays were generally formed from dispersions with number densities between 2×10^{15} and 3×10^{14} particles per cubic centimeter.

Once particle dispersions were prepared with the desired surfactant and particle concentration, transmission electron microscopy (TEM) grids were prepared. For the particle size and separation determination, grids were prepared by dropping a single drop of particle dispersion on the grid with a pipet. The Fe particles imaged in the arrays are partially oxidized because of the brief exposure during transfer to the microscope.

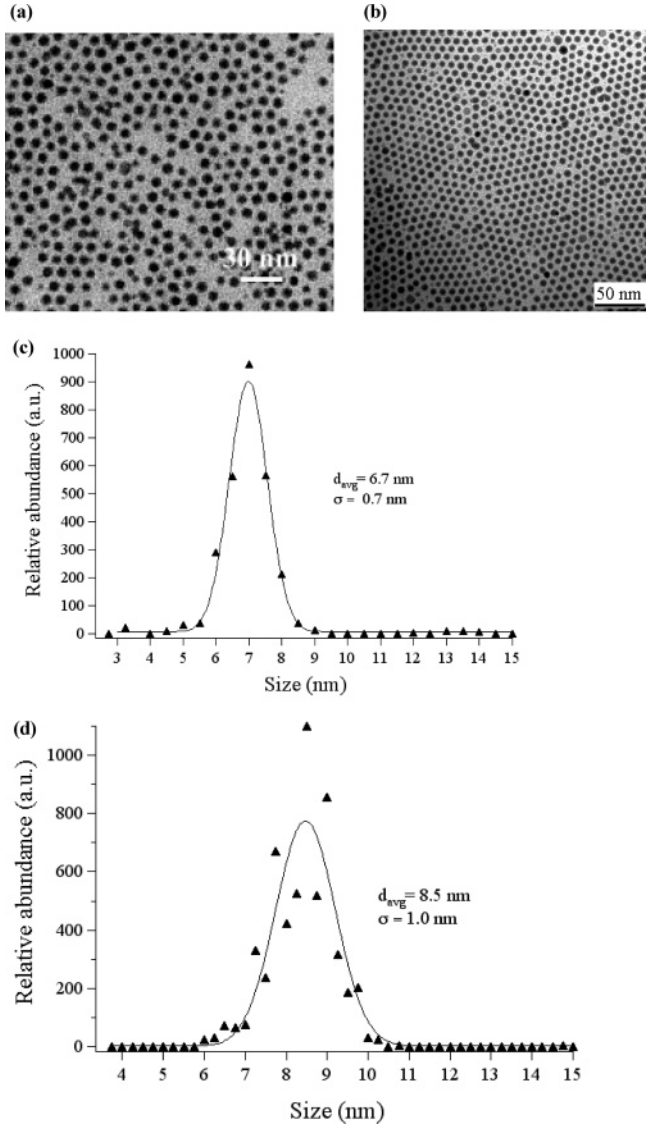

Figure 1. TEM images of (a) 6.7 ± 0.7 nm and (b) 8.5 ± 1.0 nm Fe particles coated with OA/OY. Size distributions and Gaussian fits to determine the average particle diameter and standard deviation, σ, for (c) the particles from Figure 1a, with a total of 2140 particles, and (d) for the particles from Figure 1b, with a total of 5695 particles. These data could also be fit to a log-normal function with the same average size and a normalized σ of 0.12. The "spikes" in the data arise from variations between arrays but size uniformity within an array.

The degree of oxidation can be minimized by flocculating the particles first,[33] but this makes it more difficult to determine the size and spacing information, which are critical to this study. The particle size and the separations between particles in the arrays were determined from TEM images taken with a Philips EM420 microscope operating at 120 keV. NIH Image 1.6.2 software was used to analyze the digitized images for the particle size distributions. The distributions were then fit to Gaussian functions to determine the average particle sizes and standard deviations, σ. Figure 1 shows TEM images of arrays with different particle sizes but the same edge-to-edge interparticle spacing. Figure 2 shows images of particle arrays made from the same batch of nanoparticles, but with different surfactant coatings to change the interparticle spacing. Note how the length scale of structural ordering is reduced in the sample with the shorter chain surfactant. The surfactant coating plays a significant role in the mobility of the particles during self-assembly. The images of Figures 1 and 2 are from arrays prepared by the

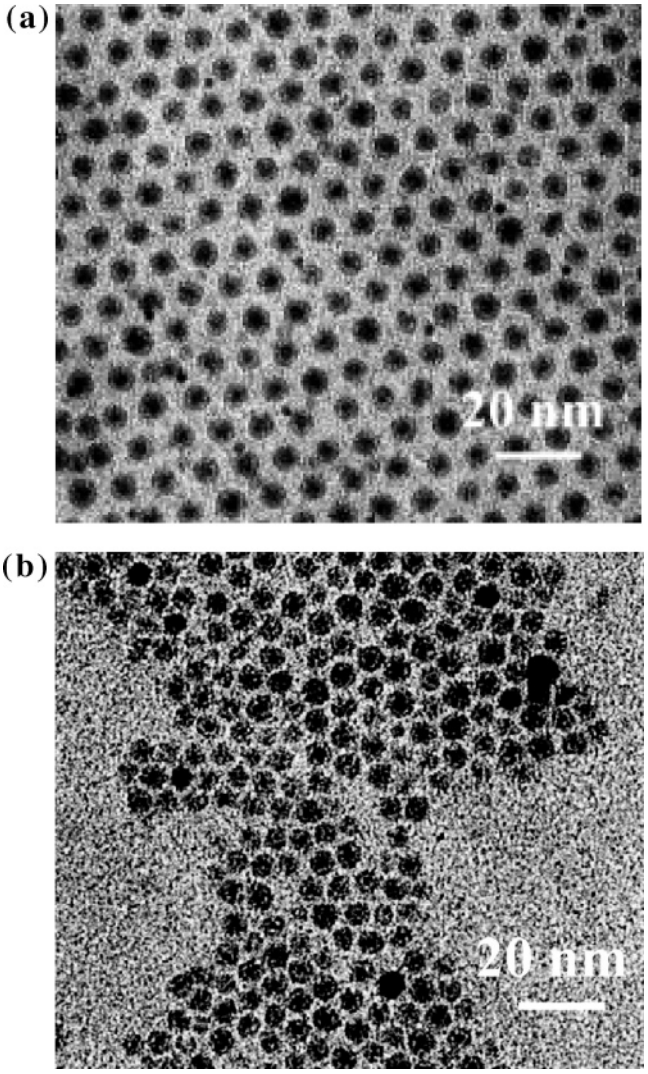

Figure 2. TEM images of 6.7 ± 0.7 nm Fe particles with different surfactant coatings. (a) Particles coated with OA/OY; (b) particles coated with HA/HY. The contraction in interparticle spacing can be seen in HA/HY-coated particles, which had an average edge-to-edge interparticle spacing of 1.2 nm, compared to 2.5 nm for the OA/OY-coated particles.

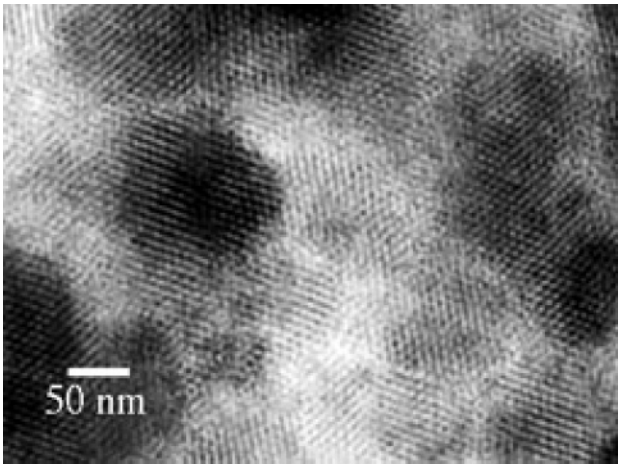

Figure 3. TEM image of nanoparticle arrays prepared by dipping into particle suspensions.

evaporation method; Figure 3 shows a typical TEM image is a dipped grid, or the sort used in magnetic measurements. Note that the length scale of the ordered regions is smaller.

B. Magnetic Measurements. Evidence for interactions between Fe nanoparticles is obtained by comparing the magnetization of samples with isolated particles with more concentrated solutions. The temperature, applied magnetic field, and time-dependent response of the magnetization all reveal different aspects of these interactions.

Magnetic measurements were done with a Quantum Design MPMS over a range of temperatures ($T = 10-300$ K) and applied fields ($H = 0-50$ kOe). This system can detect magnetic moments in the range of 10^{-5} to 1 emu with good signal-to-noise ratios. The particles used for magnetic measurements were maintained in a low oxygen environment at all times. For the magnetic studies, grids were dipped into the particle suspension using tweezers, and then held aloft in the glovebox to dry. The dip method was utilized to maximize the particle concentration. In the concentrated samples, stacks of TEM grids containing multilayer arrays, embedded in silicone grease, were used. For the dilute samples, glass ampules containing hexane dispersions were used. In all cases the diamagnetic background was subtracted.

The zero-field cooled magnetization as a function of temperature was used to identify the blocking temperature, T_B, and to identify the temperature range over which hysteresis loops and interaction effects are observable. To determine the blocking temperature, the sample was cooled in zero field from room temperature to 10 K. Once the temperature stabilized, a 100 Oe field was applied so that the magnetization would be nonzero. The moment was measured at this and subsequent higher temperatures to determine $M_{ZFC}(T)$.

For standard hysteresis loops, $M(H)$, a 50 kOe field was applied to saturate the sample, and then the magnetization was measured as the field is reduced and reversed in direction. The remanent magnetization, M_r, is the magnetization of the material following the removal of this field. The coercivity or coercive field, H_c, is the reverse field that must be applied to a previously saturated material to reduce the magnetization to zero.

In contrast with a standard hysteresis loop where the magnetization is measured at each value of the applied field H, in a remanent hysteresis loop, $M_r(H)$, the magnetization at zero field, or remanence, is measured after applying H. In the absence of an applied field, the particle moment aligns with the easy magnetization axis of the particle. In this sense, the remanent coercivity is a measure of the field necessary to flip the orientations of one-half of the moments along the easy axes. Remanent hysteresis loops are particularly useful for fine particles because they remove rotational contributions from the particles as well as any signal from paramagnetic or superparamagnetic species in the sample.

The time dependent magnetic properties were studied by applying a 50 kOe field to the sample, removing the field and measuring the remanent moment at intervals over a 10 hour period, with the first measurement taken approximately one minute after the field stabilized.

We also measured the real and imaginary parts of the AC susceptibility. The susceptibility χ is defined as M/H. Its real part χ' is the component that is in-phase with the AC driving field H, and the imaginary part χ'' corresponds to the out-of-phase component. χ'' is a maximum under conditions where the energy dissipation is greatest. Here the driving field had an amplitude of 2 Oe and the temperature ranged between 6 and 400 K.

Results

A. Dilute Dispersions. The minimum Fe particle size where appreciable interaction effects were observed in the hysteresis

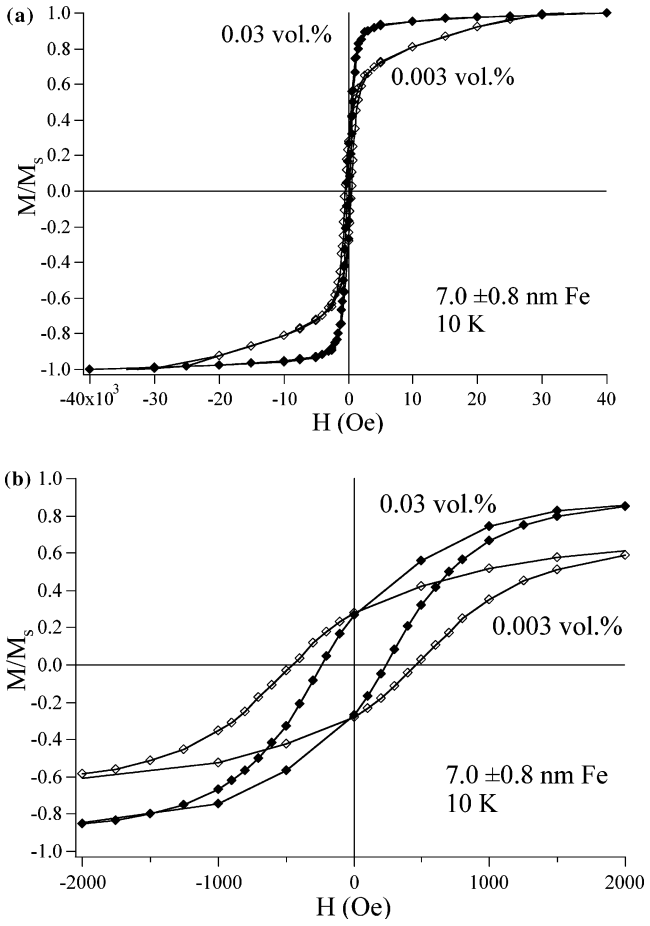

Figure 4. (a) Hysteresis loops at 10 K for 7.0 ± 0.8 nm particles frozen in hexane, for different particle concentrations; (b) Low field region of the hysteresis loops. $H_c = 240$ Oe for the 0.03 vol. % sample, and 460 Oe for the 0.003 vol. % sample.

loops was ~6 nm, though smaller moment particles have shown pronounced differences in AC susceptibility studies.[5] We compared the properties of samples of 7.0 ± 0.8 nm Fe nanoparticles dispersed in hexane with different volume fractions, ranging from 0.003 to 0.03%. This corresponds to *average* spacings between particle centers of 84 to 181 nm, which may seem sufficient to neglect particle interactions, but significant differences were observed.

For dilute dispersions of this particle size, there were only small changes in the zero field-cooled magnetization as a function of temperature. Small reductions were observed with increasing concentration, but the error in determining the peak temperature from our plots was ± 5 K, so this is only marginally significant.

Figure 4 shows the hysteresis loops. There are two main changes as the particle concentration increases: the coercivity decreases and the sample saturates at lower fields. The remanence ratio was roughly constant at 0.29, but in all cases less than the value of 0.5 expected for noninteracting uniaxial particles. For cubic materials such as Fe that have (100) easy axes, the theoretical remanence ratio is even higher, 0.8660.[33] Similar coercivity and rate of saturation trends were also seen in the remanent hysteresis loops.

The magnetic relaxation in zero field (Figure 5) shows that both samples have nearly logarithmic decay over the time window studied (approximately one minute to 10 hours, or $\sim 10^2 - 10^4$ s), and that the more concentrated sample has a slower relaxation rate. Here the sample was saturated, and then

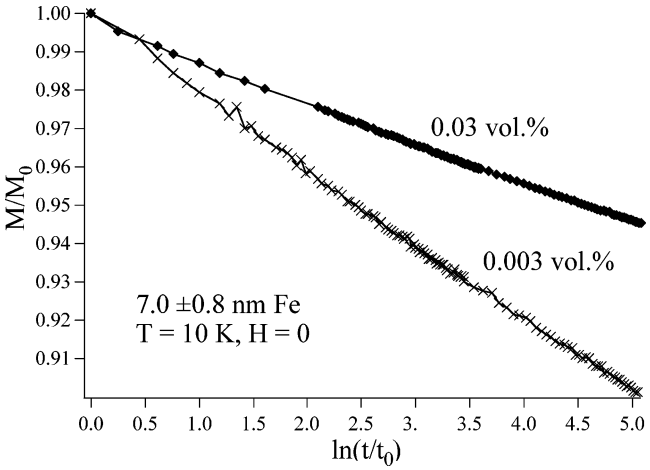

Figure 5. Magnetic relaxation as a function of time, for dilute hexane dispersions of 7.0 ± 0.8 nm particles with different volume fractions, at 10 K with $H = 0$.

TABLE 1: Comparison of Dilute Dispersions of 7.0 ± 0.8 nm Particles as a Function of Concentration

volume fraction, x_v	hysteresis loop H_c(Oe)	remanent hysteresis loop H_c(Oe)	remanence ratio, M_r/M_s	blocking temperature, T_B (K)	magnetic viscosity, S
0.0003	240	430	0.27	40	0.010
0.00003	460	720	0.29	30	0.019

the field was turned off. The data are normalized relative to the magnetization and time at the first $H = 0$ data point.

An ensemble of identical noninteracting particles is theoretically predicted to relax exponentially, with a time constant τ related to the energy barrier height, relative to the thermal energy available.[31] Here the theoretical time dependent remanence is given by $M_r = M_s \exp(-t/\tau_N)$, where the Néel decay time is defined by $\tau_N = f_0^{-1} \exp(-KV/k_BT)$, and f_0 is a constant related to the Larmor precession frequency of the magnetic moment and is on the order of 10^9 s^{-1}. In all known systems where there are detectable interactions between nanoparticles, the remanence actually decays much more slowly than in this simple model. Logarithmic decay has been reported for many systems, including magnetic recording media. This is understood in terms of a distribution of energy barriers, which may result from a distribution of particle volumes, variations in the particle orientations or local values of the magnetocrystalline anisotropy, K, or differences in the local effective field due to magnetostatic interactions. Using a simple model with a uniform energy barrier density over a finite energy width,[34] the remanence has a logarithmic time dependence, $M_r(t)/M_0 = 1 - S \ln(t/t_0)$.[35] Here M_0 is the magnetization at the time, t_0, of the first remanent measurement, and S is the characteristic slope of the decay. The magnetic viscosity, S, is 0.019 for the 0.003 vol % sample and 0.010 for the more concentrated 0.03 vol % sample. The magnetic viscosity can also be related to the distribution of energy barriers, $f(\Delta E)$, which is given by S/kT.[34,35] A large viscosity indicates a large fraction of energy barriers within the time window of the measurement. Table 1 summarizes the magnetic properties of these dilute dispersions as a function of concentration.

B. Dilute Dispersions Versus Arrays. The nanoparticle arrays obviously have far greater concentrations than the dilute dispersions, ranging from 28 to 46 vol % for the samples discussed here. Comparison of the hysteresis loop for a dispersion with that of an array made from the same particles (Figure 6) shows similar characteristics to the dilute dispersions with different concentrations, only more pronounced. The arrays

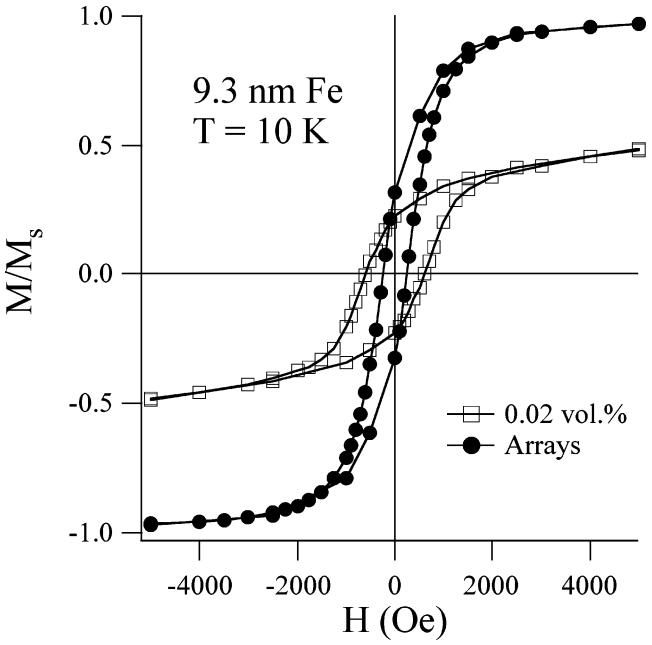

Figure 6. Hysteresis loops for 9.3 ± 1.4 nm particles, as a 0.002 vol. % solution in hexane, and in nanoparticle arrays, at 10 K. The magnetizations are normalized to the values at 50 kOe. The dilute sample has a slower approach to saturation and a higher coercivity than the arrays sample.

show much more rapid saturation than the dilute sample, and they have a smaller coercivity (250 Oe versus 600 Oe). If we compare the rate of magnetic relaxation for arrays made from the same particles in Figure 7, the viscosity increases to 0.0225. Table 2 summarizes the magnetic properties of these larger particles in dilute dispersions and in arrays.

In dilute ferrofluids there may be two peak temperatures of the imaginary AC susceptibility, χ'', but the higher temperature occurs when the fluid is in a liquid rather than frozen state and is associated with Brownian relaxation, in which the particles themselves rotate.[8] A dilute, frozen ferrofluid therefore has a single peak associated with magnetic moment rotation within the particle. Figure 8 shows the temperature dependence of M' and M'' (corresponding to χ' and χ'', respectively) for arrays of 8.5 nm nanoparticles, for two different excitation frequencies, and shows a peak plus a broad shoulder at higher temperatures. The peak temperature shifted upward from 47 ± 2 K at 1 Hz to 60 ± 5 K at 1000 Hz. There was no clear shift in the position of the shoulder. The shape of this curve reflects the distribution of energy barriers at zero field, which suggests that there are many weakly coupled particles plus a smaller proportion of more strongly coupled clusters. The upward shift in peak temperature as the frequency increases reveals that as the time scale of measurement is changed from 1 to 10^{-3} s, the proportion of particles that are blocked over that time scale increases. This is the reason that the blocking temperature that would be estimated from Figure 8a is higher than that for the SQUID magnetometer data, where the measurement time is much longer. The fact that the shoulder is insensitive to frequency indicates that its magnetization is stable over periods longer than 1 s.

C. Arrays with Different Conditions. To test for evidence of significant interactions, the same sample was first measured with the field parallel and then perpendicular to the applied field. If there were no interaction effects, the results would be identical. Because the arrays are essentially a thin film of nanoparticles, interacting particles would be expected to show shape anisotropy and should favor an in-plane magnetization.

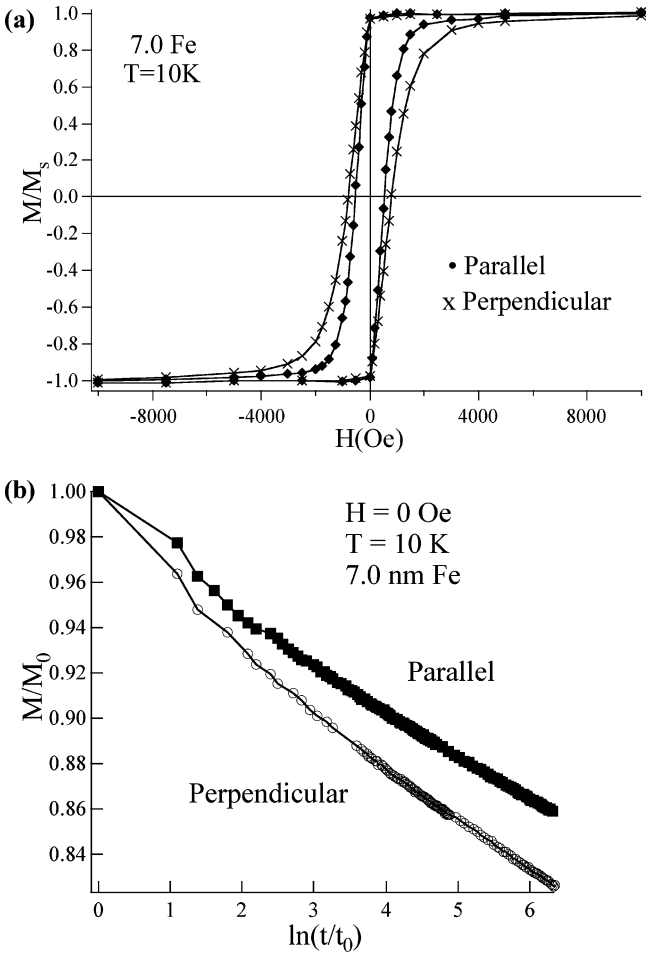

Figure 7. (a) Remanent hysteresis loops taken parallel and perpendicular to the plane of arrays of 7.0 ± 0.8 nm Fe particles; (b) Magnetic relaxation as a function of time, parallel and perpendicular to the plane of the arrays.

TABLE 2: Comparison of Dilute Dispersions and Arrays of 9.3 ± 1.4 nm Particles

volume fraction, x_v	hysteresis loop H_c(Oe)	remanent hysteresis loop H_c(Oe)	remanence ratio, M_r/M_s	blocking temperature, T_B (K)	magnetic viscosity, S
0.0002	600	850	0.20	120	0.023
0.602	400	0.32	0.32	75	0.014

Figure 7 shows remanent hysteresis loops for arrays 7.0 ± 0.8 nm particles, the same as those used for Figures 4 and 5. When the applied field is perpendicular to the plane of the arrays, there is a slower approach to saturation and a higher coercivity (450 Oe versus 330 Oe), which is consistent with a preference for in-plane magnetization. At saturation, all of the particle moments are perpendicular to the plane. When the field is reduced, interactions cause the magnetization to rotate back into the plane, and then larger fields in the opposite direction are needed to rotate them out of plane again. Figure 7b shows that the magnetic relaxation is faster when the applied field is perpendicular to the sample plane. All remaining magnetic measurements were made with the applied field parallel to the plane of the TEM grids.

Next, changes in the magnetic behavior as a function of the particle size were assessed by comparing the properties of 6.7 ± 0.7 nm and 8.5 ± 1.0 nm particles. These particles had the same oleic acid/oleylamine surfactant coating and an average edge-to-edge interparticle spacing of 2.5 nm.

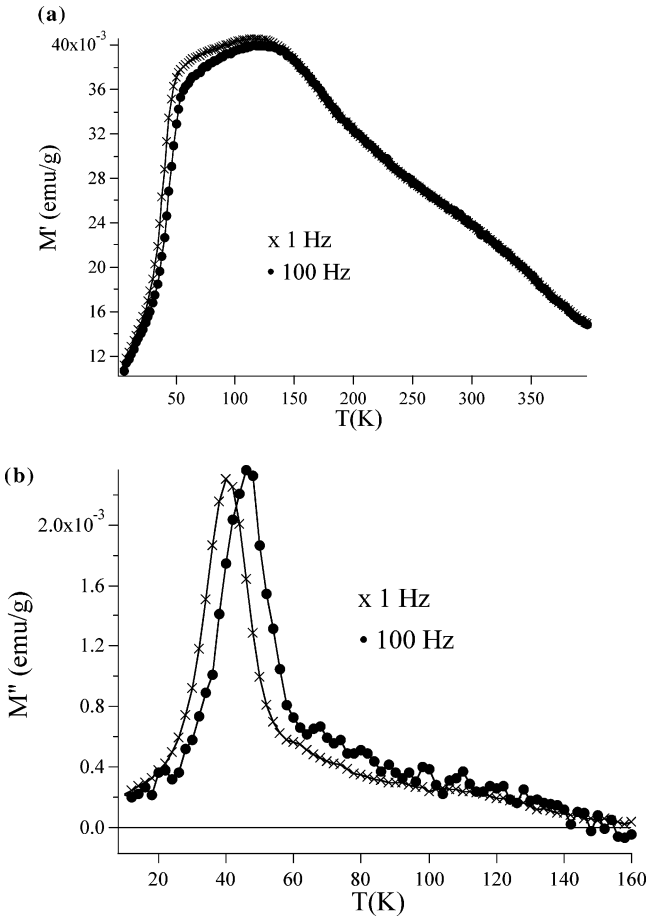

Figure 8. (a) Real part of the AC magnetization as a function of temperature, for 8.5 nm nanoparticle arrays; (b) Imaginary part of the AC magnetization.

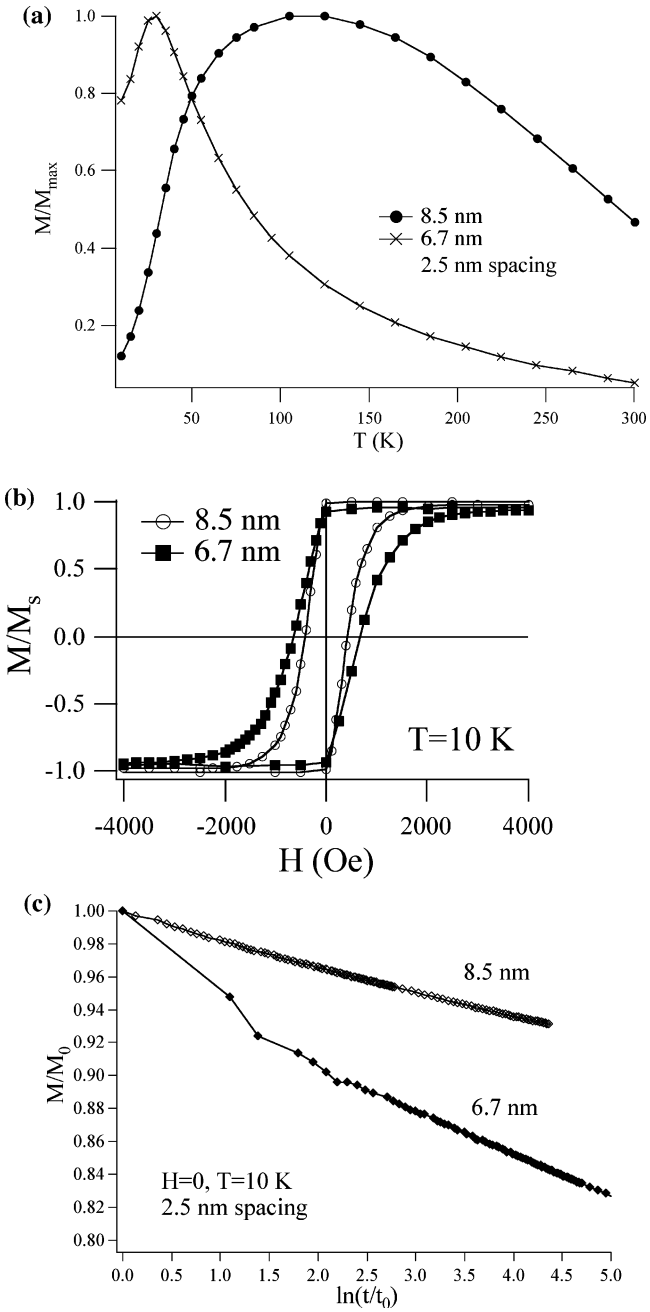

Figure 9. (a) Zero field cooled magnetization for 6.7 and 8.5 nm particles; (b) Remanent hysteresis loops; (c) Magnetic relaxation as a function of time.

Figure 9a shows that the zero field-cooled magnetization curve shifts to higher temperatures (T_B = 35 K versus 105 K) and broadens considerably. The zero field cooling freezes in a nearly random distribution of particle moments. When the field is applied at low temperature, the measured magnetization is low, unlike in the case for a bulk ferromagnet. As the temperature is increased with the field on, more and more of the particles have sufficient energy to surmount the barrier and align with the applied field, so the magnetization increases. At a certain point, the thermal energy exceeds the magnetic potential energy associated with alignment, so the moments become more disordered again and the magnetization decreases at high temperature. The zero field cooled magnetization curve will show a peak at the blocking temperature. A field cooled magnetization curve is also measured, and some groups have identified the point of deviation between the zero field cooled and field cooled curves as T_B, which typically gives slightly higher values. The field that is applied during measurement can also shift T_B; ideally the smallest field that leads to a good signal-to-noise ratio is used.

Above the blocking temperature thermal fluctuations are sufficient to randomize the magnetic moment directions within the measurement time, and they are said to be superparamagnetic. Below T_B, hysteresis is still observed and the particles are said to be blocked. This is not a true phase transition, like that between ferromagnetic and paramagnetic states at the Curie temperature, because it depends on the measurement time. For magnetometry measurements, the time between data points, τ_m, is 100 seconds, while for Mössbauer spectroscopy or neutron scattering, it is closer to a nanosecond time scale.

In dilute dispersions, the blocking temperature can be used to estimate the magnetocrystalline anisotropy, K, found from the relation $KV \approx kT\ln(\tau_m f_0) \approx 25kT$ for the measurement time of the SQUID magnetometer. Using this method, we estimated $K = 7.7 \times 10^5$ ergs/cm^3 for the 6.7 nm particles, and $K = 1.1 \times 10^6$ ergs/cm^3 for the 8.5 nm particles. The bulk value for Fe is 5.2×10^5 ergs/cm^3. Our values could be slightly higher due to their thin oxide shells (~0.5 nm).[32] K could also be overestimated because of the finite size distributions. The zero field cooled magnetization curve contribution from particles of a given size depends on the fraction of particles with that size times the particle volume, so larger particles are weighted more heavily. Simulations as a function of the normalized size distribution[36] suggest that K could be overestimated by as much

as a factor of 1.7 for the 8.5 nm particles and 1.3 for the 6.7 nm particles, based on the size distribution alone. When particles interact magnetostatically, the peak temperature of the zero field cooled magnetization may increase, but it cannot strictly be interpreted in terms of a single particle volume and anisotropy. The asymmetric nature of dipolar interactions makes it hard to treat the results in terms of an effective anisotropy, though this may be appropriate for the most dilute systems where there are only pairs of interacting particles. The changes in the zero field cooled magnetization as a function of temperature are best understood as a shift in the energy barrier distribution. Here the larger particles have on average higher energy barriers to switching, and also a broader distribution of barriers that cannot be attributed simply to the size distribution.

Remanent hysteresis loops show that the coercivity is slightly smaller for the larger particles, but the most notable different is in the rate of approach to saturation (Figure 9b). Arrays with the larger particles also have a slower rate of magnetic relaxation (Figure 9c). Over the first few data points collected, the magnetic relaxation drops sharply and then decays logarithmically. Here we have chosen M_0 and t_0 at the beginning of the logarithmic portion. In all relaxation measurements, some drop is observed due to the effect of changing the field in the magnetometer. However, this effect is particularly pronounced in the arrays and could be related to the rapid generation of flux closure pathways.

If the particle spacing is reduced from 2.5 to 1.2 nm by exchanging the oleic acid/oleylamine surfactant for hexanoic acid/hexylamine, the properties of the arrays are also modified. There is a small increase in the blocking temperature with the smaller spacing, and the zero field cooled magnetization curve is slightly broader (Figure 10a). With the reduced spacing, there is a much more gradual approach to saturation in the remanent hysteresis loop (Figure 10b). Figure 10c shows that arrays with a smaller interparticle spacing have a slightly slower magnetic relaxation rate. Table 3 summarizes the effects of changing the particle size and spacing in self-assembled arrays.

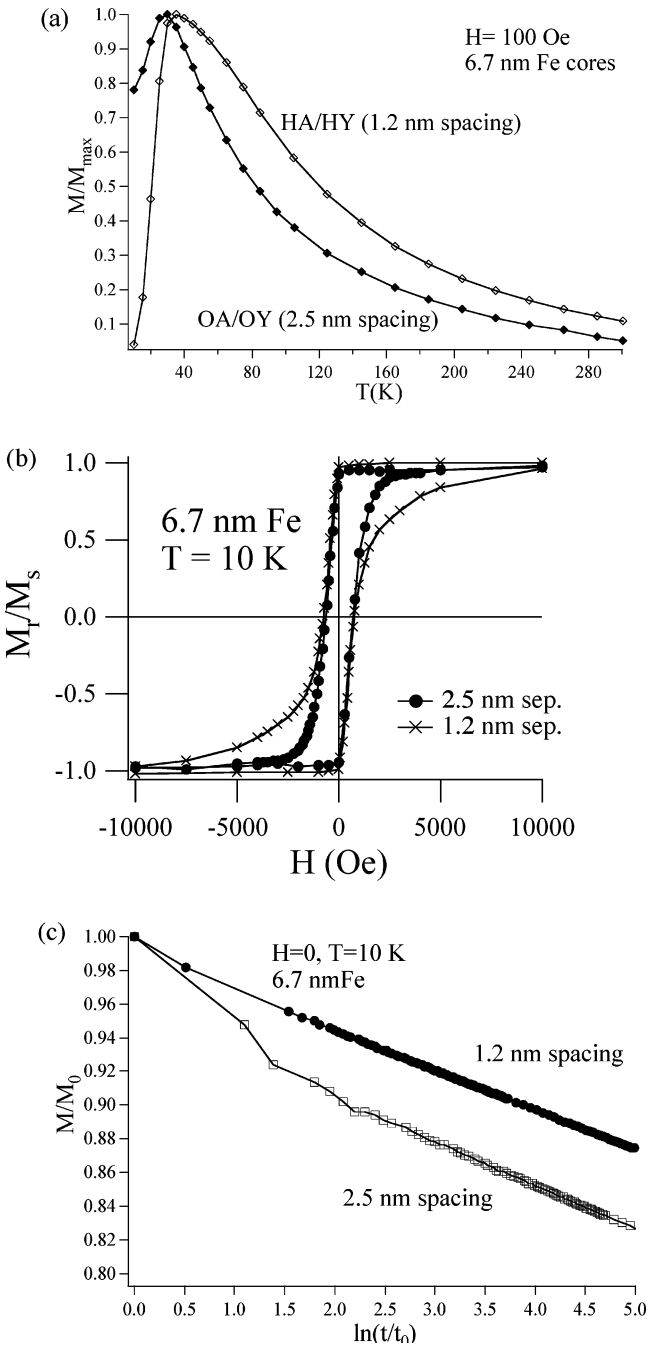

Figure 10. (a) Zero field cooled magnetization for 6.7 nm particles with average edge-to-edge inteparticle spacings of 2.5 and 1.2 nm; (b) Remanent hysteresis loops; (c) Magnetic relaxation as a function of time.

Discussion

The overall picture of magnetic interactions in dilute dispersions and nanoparticle arrays is at first confusing. In the dilute solutions, stronger interactions cause the sample to saturate at lower fields, but in the arrays higher concentrations lead to higher saturation fields. Going from a dilute to a more concentrated dispersion decreased the viscosity; however, concentrating the particles further by forming an array increases *S* again. Finally, changing the dipole energy per pair of particles in the arrays by roughly a factor of 2 leads to different results, depending on whether this is accomplished by increasing the particle size or by decreasing the interparticle spacing.

A variety of models have been used to simulate the behavior of monodomain particles based on magnetostatic interactions that modify the distribution of energy barriers to switching.[5−19] There are two main theoretical approaches to understanding magnetic nanoparticle interactions. The first builds on the statistical nature of the interactions as a function of the separation between particle moments, but does not explicitly model the positions and orientations. Some groups have used mean field methods[15,17] or an empirical Vogel−Fulcher law.[8] The interacting particles have also been treated as a cluster glass. Here the particles within a cluster switch collectively and the stability of a cluster is determined by its size, but interactions between clusters are ignored.[10−12] The second group of models explicitly monitors the moment directions within an ensemble of particles and mimimize the overall energy of the system to find the magnetic ground state.[6,7,19−21] This energy includes the sum of magnetostatic, anisotropy, and Zeemann terms. In addition to this Monte Carlo approach, Landau-Lifshitz dynamical simulations[18] have also been used to find the relaxed state configuration. As the particle assembly becomes more concentrated, the approach of these granular models becomes more important. Due to the finite volume of the particles and the preference for self-assembling into close-packed structures, the experimental distributions of particle separations may not agree with simple statistical models. In addition, there is a need for more realistic time- and temperature-dependent models in order to develop a more intuitive understanding of the complex collective behavior.

TABLE 3: Comparison of Nanoparticle Arrays with Different Particle Size and Spacing

size (nm)	avg. separation (nm)	volume fraction, x_v	hysteresis loop H_c(Oe)	remanent hysteresis loop H_c(Oe)	remanence ratio, M_r/M_s	blocking temperature, T_B (K)	magnetic viscosity, S
6.7	2.5	0.280	300	660	0.31	35	0.025
6.7	1.2	0.458	415	760	0.35	45	0.028
8.5	2.5	0.460	250	400	0.32	105	0.013

TABLE 4: Comparison of Magnetostatic and Anisotropy Energies

size (nm)	avg. sep. (nm)	vol. fraction, x_v	V_{pt} (10^{-20} cm^3)	μ_{pt} (10^{-17} emu)	E_{ms} (10^{-15} ergs)	K (10^4 ergs/cm^3)	E_K (10^{-15} ergs)	E_{ms}/E_K
5.0 [1]	69	0.0002	6.54	2.8	0.028	2.3	1.50	0.02
7.0 ± 0.8	84	0.0003	18.0	24.5	1.26	64	115	0.011
7.0 ± 0.8	182	0.00003	18.0	24.5	0.13	64	115	0.001
9.3 ± 1.4	128	0.0002	42.1	65.7	258	98	413	0.006
6.7 ± 0.7	9.5	0.280	15.8	21.5	722	64	101	7.16
6.7 ± 0.7	7.9	0.458	15.8	21.5	1180	64	101	11.7
8.5 ± 1.0	10.0	0.460	32.2	43.9	2421	97	310	7.80

Experimentally there is consensus that time-dependent quantities such as the AC susceptibility and magnetic viscosity are especially sensitive to interactions. However, there are conflicting reports about whether the coercivity and the remanence ratio, M_r/M_s, will increase or decrease with stronger interactions. Unfortunately, there have been fewer studies of interaction effects on the shape of hysteresis loops. Because the energy barriers will change as the applied field magnitude increases, this is a much more challenging problem to solve.

A particularly enlightening paper by Kechrakos and Trohidou uses Monte Carlo methods to simulate the coercivity and remanence at different temperatures.[19] These results were scaled as a function of the ratio of the dipolar and magnetocrystalline anisotropy energies. The magnetostatic energy in different systems was compared using values of the energy per pair of aligned dipoles, given by $E_{ms} = \mu_{pt}^2/4\pi a^3$, where $\mu_{pt} = M_s V$ is the particle moment and a is the center-to-center separation. In Figure 9 the magnetic properties of samples with different particle size are compared. Here E_{ms} varies by a factor of 1.7. Figure 10 shows data for samples with different interparticle separation, where E_{ms} is changed by a factor of 2.0. The anisotropy energy was given by $E_K = KV$, where K is the magnetocrystalline anisotropy and V is the particle volume. Particles were placed in random but nonoverlapping positions, and the magnetic properties were simulated both with and without periodic boundary conditions. When these authors compared their results with previous experimental findings, however, they used a different expression for the magnetostatic energy, $E_{ms} = \mu_{pt}^2/d^3$, where d is the particle diameter. In a dilute, frozen ferrofluid $d \ll a$, and this greatly overestimates the relative strength of magnetostatic interactions. Table 4 shows the values of $E_{ms} = \mu_{pt}^2/a^3$ and E_K for one of the dilute dispersions discussed by Kechrakos and Trohidou[5,15] and for the different dispersions and nanoparticle arrays whose properties are shown in Figures 4 through 10. Our data show a range of 4 orders of magnitude in the ratio of E_{ms}/E_K, and over 4 orders of magnitude in the magnetic volume fraction, making it a good test of theoretical predictions.

Figure 11 shows a schematic plot that compares the predicted coercivity as a function of the volume fraction from Kechrakos and Trohidou. On the sides of the plot we indicate the regions spanned by our experimental results. For the dilute dispersions $E_K > E_{ms}$, and under these conditions the coercivity is predicted to drop slightly with increasing concentration. Figures 4 and 6 show that our data agree. The arrays have higher volume fractions than the dilute dispersion and also have $E_{ms} > E_K$.

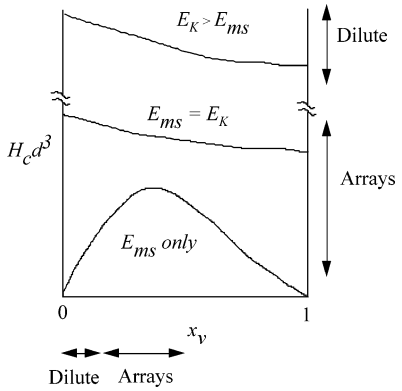

Figure 11. Coercivity multiplied by the cube of the particle core diameter, as a function of the magnetic volume fraction, x_v. (After reference 19.)

From the schematic plot, they are correctly predicted to have lower coercivities. Our data from Table 4 indicate that we are somewhere between the regimes where there are only magnetostatic interactions and where the magnetostatic and anisotropy energies are equal, so that the coercivity could either rise or drop as the volume fraction increases. We find that as the separation is reduced, so that E_K is constant while E_{ms} increases and $E_{ms}/E_K > 1$, that the coercivity rises slightly. However, for comparable changes in the volume fraction, when both E_K and E_{ms} increase, H_c drops, but the schematic suggests that it should not. The behavior of the coercivity is quite complex, and this may not be the most useful parameter to reveal interaction effects in concentrated samples.

Figure 12 shows a schematic predicting the behavior of the remanence ratio as a function of the ratio of the thermal and anisotropy energies. This predicts a higher remanence ratio for dilute samples than for arrays of the same particles, since E_K dominates for the former and E_{ms} for the latter. While demagnetizing interaction causes lower remanence ratios than predicted for noninteracting particles, we observe that this ratio increases with stronger interactions. It predicts higher blocking temperatures for the arrays, which have been reported by several groups.[15,25,26] It also predicts a relative insensitivity to the concentration above a fraction of 0.16, which may partly explain why the blocking temperature changes only slightly between the 6.7 nm samples with different spacings. When we change the magnetic volume fraction by roughly the same amount by changing the particle size, this simultaneously increases the anisotropy energy 3-fold. In a plot of the remanence ratio versus

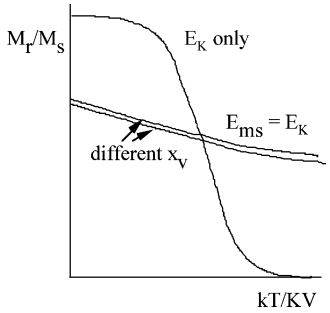

Figure 12. The remanence ratio as a function of the ratio between the thermal and anisotropy energies, for different values of the relative magnetostatic and anisotropy energies. (After reference 19.) If the magnetostatic and anisotropy energies are comparable, the remanence ratio is only weakly dependent on the magnetic volume fraction, x_v.

temperature, this would be equivalent to having a higher blocking temperature in the larger particles, as we observe (Figure 9a).

In addition to agreeing with much of the behavior predicted based on the ratio of the magnetostatic and anisotropy energies, our data show new features that are not as well understood. The broadening of the zero field cooled magnetization curve is a signature of collective behavior, but it is less clear whether the arrays are a true dipolar ferromagnet, such as that predicted by Luttinger and Tisza,[27] or if they are an assembly of interacting blocked particles without any domain structure. At low enough temperatures and short enough times, they will be ferromagnetic, but here we consider the time and temperature scales of our measurements ($T \geq 10$ K, $t \geq 1$ min). The arrays are not dilute enough to have a sharp cusp in the magnetization versus temperature curve, but they likely contain clusters of coupled particle moments over a range of sizes. This makes them "spin glass-like" rather than a true spin glass. The cluster relaxation rates are still perturbed by the magnetization states of nearby clusters, but not all scaling relations and critical exponents apply.

The degree of structural disorder has been shown to affect the rate of relaxation,[25,26] but since the arrays studied here were made with the same evaporative self-assembly method, we assume that all of them have considerable disorder like that shown in Figure 3. We note a marked difference in the rate of approach to saturation in both the ordinary and remanent hysteresis loops, as seen in Figures 4, 6, 7, 9, and 10. These differences are more pronounced for the remanent loops, which can be viewed as the integral of the switching field distributions. This is also a reflection of the change in the energy barrier distribution, but, unlike with the magnetic relaxation measurements, these barriers are field-dependent.

Consider first the particle moments in a highly diluted dispersion, well below the blocking temperature. If $H = 0$, the particle moments will lie along easy axes, and the magnetocrystalline anisotropy will determine the energy barrier height for magnetization reversal, and the measured magnetic properties will agree with Stoner−Wohlfarth theory for noninteracting particles. If the concentration is increased so that particles begin to interact with each other, then the anisotropy is modified by the field of the surrounding particle moments. The effective anisotropy can be viewed as the energetic preference for a particle to be magnetized in a particular direction. The net magnetostatic field from other particles is likely to be misaligned, relative to the easy axes of the particle, and so the effect is to reduce the effective anisotropy, relative to K_{mx}. This will lead to reduced values of the coercivity, as observed. The interactions will also couple moments from different particles so that they switch together, and with the reduced H_c, this leads to a lower field being required for saturation. Because the particle moments are stabilized by the fields from their neighbors, the magnetic relaxation in zero field is slower, as seen in Figure 5.

If we argue that the main effect of increasing the concentration in dilute dispersions is to favor ferromagnetic interactions of small numbers of particles, we must consider why the remanence ratio of the dispersions is well below the statistically predicted values. Dynamic light scattering has shown evidence of particle clustering, even in fairly dilute liquid dispersions,[32] so the properties may in fact be dominated by separations well below the statistical average spacing. Both the ability of the solvent to stabilize the dispersion and possible phase separation upon freezing may lead to nonstatistical distributions of particle separations.

The experimental distribution of switching fields is proportional to the derivative of a remanent hysteresis loop, $dM_r(H)/dH$, which is known as the irreversible susceptibility, χ_{irr}. χ_{irr} and S are related by the fluctuation field, H_f, such that $H_f = SM_0/\chi_{irr}$.[35] H_f is in turn sometimes associated with a switching volume, V. Here $H_f = kT/M_sV$, and V is not necessarily equal to the particle volume.[7] Using these relations with our experimental data, we find switching volumes smaller than the particle volumes, and so this approach reveals little about the coupled cluster sizes.

For the dilute dispersions, the effect of magnetostatic coupling is effectively to introduce anisotropy, in terms of a preference for being magnetized in a particular direction at zero applied field. When the particles are concentrated, the effective magnetostatic field is more appropriately viewed as arising from the Lorentz cavity field from many particles.[19] This is analogous to the exchange-based magnetic interactions in magnetic alloys such as Au:Fe and Cu:Mn as a function of the concentration of magnetic atoms. At concentrations below ~10 at. %, the alloy is a spin glass containing single spins and small isolated clusters. As the concentration increases, but below the percolation threshold, the alloy is known as a cluster glass or mictomagnet, with large interacting clusters but no long-range behavior.[37] The behavior of cluster glasses is still not well understood. The clusters of coupled spins in the nanoparticle arrays are likely to be larger than in the dilute ferrofluids, and the fields they generate at the positions of other coupled clusters are likely to be stronger. A cluster with a larger number of parallel spins will have a higher switching field, just as the barrier for magnetization reversal of a single particle increases with the number of spins (i.e., with its volume). The arrays are likely to have a much broader range of barrier heights because of the possibility of many different cluster sizes. The field at a particular particle will change as its neighbors reverse their magnetization directions, and so the energy barrier distribution will evolve, either as the applied field is varied in a hysteresis loop, or as time increases in magnetic relaxation, or as the temperature increases in zero field cooled magnetization measurements. The reversal of some clusters at low applied fields or short times could then increase the barriers for reversal of the remaining clusters. This could explain the slower rates of approach to saturation with the more strongly interacting particles and why this feature is so much more pronounced than the changes in H_c, as seen in Figures 9b and 10b. Half the magnetic volume has a lower switching field than H_c, but the coercivity is not necessarily the *average* switching field. This could also explain the lower magnetic relaxation rates with stronger interaction strength in the arrays (Figure 9c and 10c).

Conclusions and Future Directions

In all cases we observe a reduced remanence ratio, relative to the theoretical value for noninteracting particles, which indicates that *at zero field* the overall interactions are primarily demagnetizing. However, with increasing concentration the degree of demagnetization weakens. The hysteresis loops all show two different regimes: a rapid change in the magnetization near the coercivity and a gradual approach to saturation. For the most part, the coercivity drops as the volume fraction increases. The rate of approach to saturation shows more complex behavior, first increasing with more concentrated dispersions, and when moving from dispersions to arrays, but then decreasing when the strength of the magnetostatic interactions within the arrays is further increased. The magnetic relaxation at zero field shows logarithmic decay regions for all samples. The magnetic viscosity associated with this decay increases with concentration for the dilute dispersions, but decreases for arrays made from larger particles that have higher blocking temperatures, and therefore higher anisotropy energies. The peak temperatures of the zero field cooled magnetization showed modest reductions in the arrays, relative to the blocking temperatures of dilute dispersions of the same particles. The imaginary part of the AC susceptibility shows an additional shoulder at higher temperature, in addition to the loss peak similar to that in a dilute ferrofluid. The insensitivity to frequency indicates that there are magnetic regions that are stable on a time scale of 1 s or longer.

In a simplified picture of dilute dispersions with weak interactions, the effect of the dipolar field is to generate an effective anisotropy in clusters with small numbers of particles. They are strongly coupled to each other and weakly coupled to other clusters. The reversal of spins in one cluster does not significantly affect the state of spins in another, over the time and temperature ranges studied here. These frozen ferrofluids act as ensembles of weakly interacting particle clusters, rather than as a dipolar ferromagnet. In a dense assembly such as the self-assembled nanoparticle arrays, however, magnetostatic interactions between neighboring clusters will affect the local demagnetizing field. It is feasible that in intermediate applied fields a domain-like structure develops within the arrays that contains flux closure pathways and therefore stabilizes some of the particle moments against switching.

Unlike in magnetic−nonmagnetic metal alloys that have exchange coupling, we cannot compare with the bulk Curie temperature. It is therefore difficult to determine the concentration at which the cluster glass transforms into a dipolar ferromagnet, with long-range order that is stable over time. Our magnetic relaxation results show a significant remanent magnetization 10 hours after the applied field is removed, at 10 K, so we have made samples with magnetic stability. However, we cannot yet determine the nanoscale magnetization pattern within the array. The AC susceptibility data suggest that a small fraction of the particles within the array samples may be responsible. Small angle neutron scattering experiments are under way to determine the magnetic coherence lengths in the arrays.

There are a number of interesting directions for future work on magnetic nanoparticle interactions. As we have demonstrated, even with narrow size distributions and good control of the interparticle spacing, it is difficult to make quantitative predictions of the magnetic properties. On the synthetic front, there is a need to prepare macroscopic samples with even greater structural uniformity. Here the growth of nanoparticle crystals through the slow diffusion of a poorly coordinating solvent,[38]

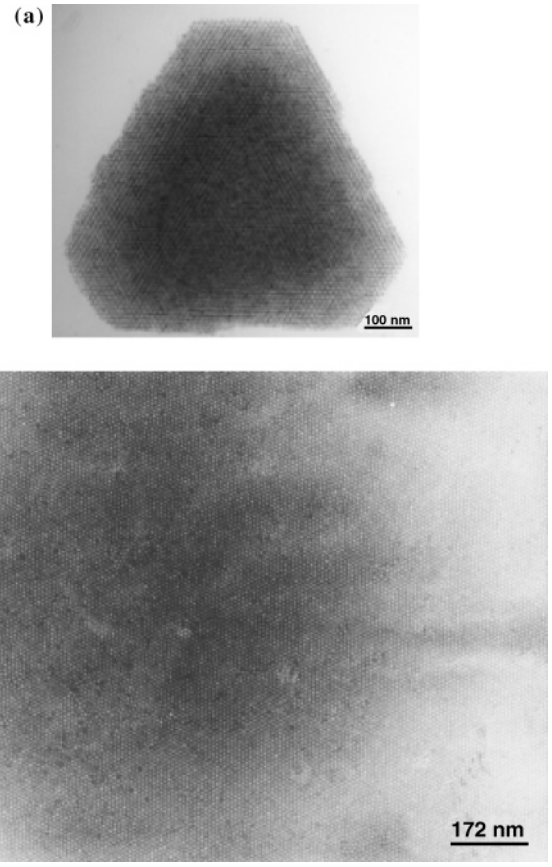

Figure 13. Uniform structures grown with 7.0 nm Co nanoparticles. (a) Faceted nanoparticle crystal; (b) Langmuir monolayer of 7.0 nm Co nanoparticles showing order over large areas.

the formation of large area Langmuir layers of nanoparticles (Figure 13), and the synthesis of cubic nanoparticles with controlled crystallographic orientation[39] offer promise. There is room for improvement in increasing the particle moment and decreasing the interparticle separation without sacrificing the regularity of the ordering. Improved nanoscale magnetic characterization techniques applicable to small patterned structures would be beneficial. In magnetic measurements it will be important to determine the sizes of the coupled clusters of magnetic nanoparticles and see how they vary as a function of time and temperature. These clusters correspond to the domains of a bulk ferromagnet, but little is understood about how they evolve. AC susceptibility, neutron scattering, X-ray magnetic circular dichroism, and electron holography may all be useful tools for determining the domain sizes. On the theoretical front, there is a need for improved time and temperature-dependent simulations of the magnetic switching within nanoparticle assemblies, so that the onset of collective behavior can be explored more fully. Up until now, most models have treated magnetostatic interactions as a perturbation to the behavior of isolated particles, rather than as a new form of nanocomposite ferromagnet without exchange effects. More detailed experimental and theoretical data can provide the input for the development of such a model.

Acknowledgment. S.A.M. thanks the National Science Foundation (CTS-0227645) and the Petroleum Research Fund of the American Chemical Society (ACS-PRF-37578-AC5) for financial support. Ames Laboratory is operated by Iowa State University for the Department of Energy under Contract No. W-7405-ENG-82.

References and Notes

(1) Hess, P. H.; Parker, P. H., Jr. *J. Appl. Polym. Sci.* **1966**, *10*, 1915−1927.

(2) Griffiths, C. H.; O'Horo, M. P.; Smith, T. W. *J. Appl. Phys.* **1979**, *50*, 7108.

(3) Grinstaff, M. W.; Salamon, M. B.; Suslick, K. S. *Phys. Rev. B* **1993**, *48*, 269.

(4) Park, S. J.; Kim, S.; Lee, S.; Zhim, Z. G.; Char, Kookrin; and Hyeon, T. *J. Am. Chem. Soc.* **2000**, *122*, 8581−8582.

(5) Luo, W.; Nagel, S. R.; Rosenbaum, T. F.; Rosensweig, R. E. *Phys. Rev. Lett.* **1992**, *67*, 2721−2724.

(6) Chantrell, R. W.; Fearon, M.; Wohlfarth, E. P. *Phys. Status Solidi A* **1986**, *97*, 213.

(7) O'Grady, K.; El-Hilo, M.; Chantrell, R. W. *IEEE Trans. Magn.* **1993**, *29*, 2608.

(8) Zhang, J.; Boyd, C.; Luo, W. *Phys. Rev. Lett.* **1996**, *77*, 390.

(9) Djurberg, C.; Svedlindh, P.; Nordblad, P.; Hansen, M. F.; Bødker, F.; Mørup, S. *Phys. Rev. Lett.* **1997**, *79*, 5154.

(10) Humfeld, K. D.; Giri, A. K.; Majetich, S. A.; Venturini, E. L. *IEEE Trans. Magn.* **2001**, *37*, 21994.

(11) Chamberlin, R. V.; Humfeld, K. D.; Farrell, D.; Yamamuro, S.; Ijiri, Y.; Majetich, S. A. *J. Appl. Phys.* **2001**, *91*, 6961.

(12) Chamberlin, R. V.; Hemberger, J.; Loidl, A.; Humfeld, K. D.; Farrell, D.; Yamamuro, S.; Ijiri, Y.; Majetich, S. A. *Phys. Rev. B* **2002**, *66*, 172403.

(13) Mørup, S.; Madsen, M. B.; Frank, J.; Villadsen, J.; and Koch, C. J. W. *J. Magn. Magn. Mater.* **1983**, *40*, 163.

(14) Jonsson, T.; Nordblad, P.; Svedlindh, P. *Phys. Rev. B* **1998**, *57*, 497.

(15) Dormann, J.; Bessais, L.; Fiorani, D. *J. Phys. C* **1988**, *21*, 2015.

(16) Hendriksen, P. V.; Mørup, S.; Christiansen, G.; Jacobsen, K. W. Magnetization Reversal in Clusters of Magnetic Particles, In *Science and Technology of Nanostructured Magnetic Materials*; Hadjipanayis, G., Prinz, G. A., Eds.; Plenum Press: New York, 1992; p. 573.

(17) Mørup, S.; Tronc, E. *Phys. Rev. Lett.* **1994**, *72*, 3278.

(18) Held, G. A.; Grinstein, G.; Doyle, H.; Sun, S.; Murray, C. B. *Phys. Rev. B* **2001**, *64*, 012408.

(19) Kechrakos, D.; Trohidou, K. N. *Phys. Rev. B* **1998**, *58*, 12169−12177.

(20) Petit, C.; Russier, V.; Pileni, M. P. *J. Phys. Chem. B* **2003**, *107*, 10333−10336.

(21) Russier, V.; Petit, C.; Legrand, J.; Pileni, M. P. *Phys. Rev. B* **2000**, *62*, 3910.

(22) Lalatonne, Y.; Motte, L.; Russier, V.; Ngo, A. T.; Bonville, P.; Pileni, M. P. *J. Phys. Chem. B* **2004**, *108*, 1848−1854.

(23) Puntes, V. F.; Krishnan, K. M. *IEEE Trans. Magn.* **2001**, *37*, 2210.

(24) Garcia-Otero, J.; Porto, M.; Rivas, J.; Bunde, A. *Phys. Rev. Lett.* **2000**, *84*, 167−170.

(25) Farrell, D.; Ding, Y.; Sanchez-Hanke, C.; Kao, C.-C.; Majetich, S. A. *J. Appl. Phys.* **2004**, *95*, 6636.

(26) Farrell, D.; Cheng, Y.; Ding, Y.; Yamamuro, S.; Sanchez-Hanke, C.; Kao, C.-C.; Majetich, S. A. *J. Magn. Magn. Mater.* **2004**, *282*, 1−5.

(27) Luttinger, J. M.; Tisza, L. *Phys. Rev.* **1946**, *70*, 954

(28) Stoner, E. C.; Wohlfarth, E. P. *Trans. R. Soc. London* **1948**, *A240*, 599.

(29) Brown, W. F., Jr. *J. Appl. Phys.* **1959**, *30S*, 130S.

(30) Meikeljohn, W. H.; Bean, C. P. *Phys. Rev.* **1956**, *102*, 1413.

(31) Néel, L. *Ann. Géophys.* **1949**, *5*, 99.

(32) Street, R.; Woolley, J. C. *Proc. Phys. Soc. A* **1949**, *62*, 562.

(33) Farrell, D.; Majetich, S. A.; Wilcoxon, J. P. *J. Phys. Chem. B* **2003**, *107*, 11022.

(34) Chikazumi, S. *Physics of Magnetism*; John Wiley and Sons: New York, 1964; p. 100.

(35) An alternative expression is sometimes used for the magnetic viscosity, $M(t) = M_o - S \ln t$. This leads to viscosities with awkward units, and we therefore use the dimensionless version.

(36) Sappey, R.; Vincent, E.; Hadacek, N.; Chaput, F.; Boilot, J. P.; Zins, D. *Phys. Rev. B* **1997**, *56*, 14551.

(37) Mydosh, J. A. *Spin Glasses: An Experimental Introduction*; Taylor and Francis: London, Washington, DC, 1993; p. 36.

(38) Talapin, D. V.; Shevchenko, E. V.; Kornowski, A.; Gaponik, N.; Haase, M.; Rogach, A. L.; Weller, H. *Adv. Mater.* **2001**, *13*, 1868.

(39) Dumestre, F.; Chaudret, B.; Amiens, C.; Renaud, P.; Fejes, P. *Science* **2004**, *303*, 821−823.